Molecular Biology of the Cell
Vol. 15, 1969–1980, April 2004

Calcium Signaling Is Involved in Dynein-dependent Microtubule Organization

L'ubica Adamíková,* Anne Straube,† Irene Schulz,‡ and Gero Steinberg§

Max-Planck-Institut für terrestrische Mikrobiologie, Karl-von-Frisch-Straβe, D-35043 Marburg, Germany

Submitted September 17, 2003; Revised December 22, 2003; Accepted December 27, 2003
Monitoring Editor: David Drubin

The microtubule cytoskeleton supports cellular morphogenesis and polar growth, but the underlying mechanisms are not understood. In a screen for morphology mutants defective in microtubule organization in the fungus *Ustilago maydis*, we identified *eca1* that encodes a sarcoplasmic/endoplasmic calcium ATPase. *Eca*1 resides in the endoplasmic reticulum and restores growth of a yeast mutant defective in calcium homeostasis. Deletion of *eca1* resulted in elevated cytosolic calcium levels and a severe growth and morphology defect. While F-actin and myosin V distribution is unaffected, Δ*eca1* mutants contain longer and disorganized microtubules that show increased rescue and reduced catastrophe frequencies. Morphology can be restored by inhibition of Ca^{2+}/calmodulin-dependent kinases or destabilizing microtubules, indicating that calcium-dependent alterations in dynamic instability are a major cause of the growth defect. Interestingly, dynein mutants show virtually identical changes in microtubule dynamics and dynein-dependent ER motility was drastically decreased in Δ*eca1*. This indicates a connection between calcium signaling, dynein, and microtubule organization in morphogenesis of *U. maydis*.

INTRODUCTION

Calcium (Ca^{2+}) plays a key role in signal transduction in eukaryotic cells. A transient elevation in cytosolic Ca^{2+} stimulates several Ca^{2+} binding proteins that elicit downstream signaling pathways (Stull, 2001). Ubiquitous effectors of Ca^{2+} signaling are Ca^{2+}/calmodulin-dependent protein kinases (CaMKs) and the Ca^{2+}/CaM-dependent phosphatase calcineurin, which act by modulating the phosphorylation state of several proteins. The Ca^{2+} signal terminates when Ca^{2+}-ATPases and Ca^{2+}/H^{+} exchangers transport Ca^{2+} out of the cell or sequester it into organelles, thereby reducing cytosolic Ca^{2+} concentration to basal levels. The endoplasmic reticulum (ER) is the major Ca^{2+} store in most eukaryotic cells and sarco/ER-resident Ca^{2+}-ATPases (SERCA; East, 2000) are required to pump Ca^{2+} into the ER so as to maintain low resting levels of cytosolic Ca^{2+} and to activate Ca^{2+} binding chaperones that assist the folding and modification of secretory proteins (Corbett and Michalak, 2000).

There is a growing body of evidence demonstrating a requirement for Ca^{2+}-dependent signaling during the infection or invasion phase in diverse parasites of plants and animals, such as *Histoplasma capsulatum* (Sebghati *et al*., 2000) and *Cryptococcus neoformans* (Fox and Heitman, 2002). In particular, recent work in fungal pathogens reveals that inhibiting the function of calcineurin and Ca^{2+}/CaMKs has major effects on fungal growth and leads to a loss in virulence (Joseph and Means, 2000; Cruz *et al*., 2002). Comparable pathways implicating Ca^{2+} signaling in the regulation of growth cone extension and filopodial motility in mammalian cells have been described (Gomez and Spitzer, 1999), suggesting that the role of Ca^{2+} in regulating morphogenesis is of widespread relevance. A potential target of Ca^{2+} signaling is the cytoskeleton that supports polar growth and determines the morphology of the cell. CaMKs are thought to regulate the activity of actin-based myosin V (Karcher *et al*., 2001). In addition, it has been shown that altered calcium homeostasis affects morphology and microtubule (MT) dynamics in fission yeast (Facanha *et al*., 2002), and CaMKs might also be involved, because it was shown that they regulate MT dynamics by phosphorylation of the MT regulator stathmin (Gardin *et al*., 1997).

Here, we describe a role of calcium in morphogenesis of the corn smut fungus, *Ustilago maydis*. This model pathogen is amenable to molecular genetics, its genome is published, and it is perfectly suited to analyze fungal dimorphism and pathogenicity (Bölker, 2001). Furthermore, it deserves attention because it shares similarities with vertebrate systems in several aspects of its cell biology, including unexpected gene conservation with higher eukaryotes (Kojic *et al*., 2002), a highly dynamic MT cytoskeleton (Steinberg *et al*., 2001; Straube *et al*., 2003), and the existence of kinesin motors, such as Kif1A- and a conventional kinesin (Lehmler *et al*., 1997; Wedlich-Söldner *et al*., 2002b), which are also crucial for axonal transport (Hirokawa, 1998). Moreover, similar to vertebrate cells intracellular motility of endosomes and ER depends on MTs and associated dynein (Wedlich-Söldner *et al*., 2000, 2002a).

Article published online ahead of print. Mol. Biol. Cell 10.1091/mbc.E03–09–0675. Article and publication date are available at www.molbiolcell.org/cgi/doi/10.1091/mbc.E03–09–0675.

Present addresses: *Hanulova 1, 84101 Bratislava, Slovakia; †Wellcome Trust Centre for Cell Biology, ICMB, University of Edinburgh, King's Buildings, Edinburgh EH9 3JR, Scotland, UK; ‡Institut für Zellbiologie, LMU, Schillerstr. 42, D-80336 München, Germany.

§Corresponding author. E-mail address: gero.steinberg@staff.uni-marburg.de.

Abbreviations used: CaM, calmodulin; CaMK, Ca^{2+}-calmodulin–dependent kinase; ER, endoplasmic reticulum; CFP, cyan fluorescent protein; GFP, green fluorescent protein; MT, microtubule; SERCA, sarcoplasmic/endoplasmic reticulum Ca^{2+} ATPase; *ts*, temperature sensitive; YFP, yellow fluorescent protein.

Table 1. Strains and plasmids used in this study

Strains/plasmids	Genotype	Reference
FB1	*a1b1*	Banuett and Herskowitz, 1989
FB2	*a2b2*	Banuett and Herskowitz, 1989
FB1Eca1^{ts}	*a1b1 eca1*$_{A1576T}$	This study
FB1Eca1^{ts}EG	*a1b1 eca1*$_{A1576T}$/pEca1GFP	This study
FB2EYEC	*a2b2*/pEca1YFP/pERCFP	This study
FB2ΔEca1	*a2b2* Δ*ecal*::*ble*^{R}	This study
K616	*MATa pmr1*::*HIS3 pmc1*::*TRP1 cnb1*::*LEU2 ura3*	Cunningham and Fink, 1994
K616pGal	*MATa pmr1*::*HIS3 pmc1*::*TRP1 cnb1*::*LEU2 ura3*/pGal	This study
K616Eca1	*MATa pmr1*::*HIS3 pmc1*::*TRP1 cnb1*::*LEU2 ura3*/pGEca1	This study
K616Eca1Y	*MATa pmr1*::*HIS3 pmc1*::*TRP1 cnb1*::*LEU2 ura3*/pGEca1YFP	This study
FB1YFP	*a1b1*/pOYFP	This study
FB2CMP	*a2b2*/pCaMP	This study
FB2ΔEca1CMP	*a2b2* Δ*eca1*::*ble*^{R}pCaMP	This study
FB2ΔEca1GT	*a2b2* Δ*ecal*::*ble*^{R}/potefGFPTub1	This study
FB1GT	*a1b1*/potefGFPTub1	Steinberg *et al*., 2001
FB2GT	*a2b2*/potefGFPTub1	This study
FB1Dyn2^{ts}	*a1b1* Δ*dyn2*::*dyn2*^{ts}, *nat*^{R}	Wedlich-Söldner *et al*. 2002a
FB1Dyn2^{ts}GT	*a1b1* Δ*dyn2*::*dyn2*^{ts}, *nat*^{R}/potefGFPTub1	This study
FB2ΔEca1GM	*a2b2* Δ*eca1*::*ble*^{R}/pOGmyo5C	This study
FB2EG	*a2b2*/pERGFP	This study
FB2ΔEca1EG	*a2b2* Δ*ecal*::*ble*^{R}/pERGFP	This study
FB1Dyn2^{ts}EG	*a1b1* Δ*dyn2*::*dyn2*^{ts}, *nat*^{R}/pERGFP	Wedlich-Söldner *et al*. 2002a
FB2ΔEca1Dyn2^{ts}	*a2b2* Δ*eca1*::*ble*^{R}, Δ*dyn2*::*dyn2*^{ts}, *nat*^{R}	This study
FB2ΔEca1Dyn2^{ts}GT	*a2b2* Δ*eca1*::*ble*^{R}, Δ*dyn2*::*dyn2*^{ts}, *nat*^{R}/potefGFPTub1	This study
pEca1GFP	P*eca1-eca1-egfp*, *cbx*^{R}	This study
pEca1YFP	P*eca1-eca-yfp*, *ble*^{R}	This study
pERCFP	P*otef-cal*^{S}*-cfp-HDEL*, *cbx*^{R}	Böhnert *et al*. unpublished
pGal	P*gal*$_{1-10}$, *URA3*	H. Ullrich, unpublished
pGEca1	P*gal*$_{1-10}$*-ecal*, *URA3*	This study
pGEca1YFP	P*gal*$_{1-10}$*-ecal-YFP*, *URA3*	This study
pOYFP	P*otef-yfp*, *cbx*^{R}	This study
pCaMP	P*otef-M13-cpEGFP-CaM*, *cbx*^{R}	This study
pOGmyo5C	P*otef-egfp-myo5*, *cbx*^{R}	Weber *et al*., 2003
pERGFP	P*otef-cal*^{S}*-egfp-HDEL*, *cbx*^{R}	Wedlich-Söldner *et al*., 2002a
potefGFPTub1	P*otef-egfp-tub1*, *cbx*^{R}	Steinberg *et al*. 2001

a, *b*, mating type loci; Δ, deletion; P, promoter; ::, homologous replacement; −, fusion; *ble*^{R}, phleomycine resistance; *cbx*^{R}, carboxin resistance; *nat*^{R}, nourseothricin resistance; /, ectopically integrated; *egfp*, enhanced green fluorescent protein; *yfp/cfp*, yellow-shifted/cyan-shifted fluorescent protein; *A1576T*, point mutation at nucleotide residue +1576; *cal*^{S}, signal sequence of calreticulin from rabbit (nt1-51); *HDEL*, ER retention signal; *M13-cpEGFP-CaM*, GFP-based Ca^{2+} probe (Nakai *et al*., 2001).

As an initial step toward elucidating the role of Ca^{2+} signaling in morphogenesis in this fungus, we have characterized *eca1*, which was isolated by complementing a temperature-sensitive (*ts*) mutant. We show that *Eca*1 represents a true SERCA that is required for proper growth and cell survival. At standard growth conditions, mutants show a defective cell morphology that most likely results from altered MT dynamics and organization. Detailed analysis of parameters of MT dynamic instability, as well as ER motility suggests an involvement of cytoplasmic dynein in the Δ*eca1* phenotype. Both the morphology phenotype and MT defect can be rescued by inhibition of CaM-kinases, whereas inhibition of the Ca^{2+}-dependent phosphatase calcineurin aggravated the phenotype of Δ*eca1* mutants.

MATERIALS AND METHODS

Generation of Mutants and Identification of eca1

Wild-type strain FB1 was UV-mutagenized to a survival rate of 4–5% and *ts* mutants were identified by growth at 24 and 34°C. One mutant was complemented with a genomic library on a self-replicating plasmid. Two plasmids contained a complementing 5.5-kb *Hind*III fragment that was cloned and sequenced with standard methods, revealing a single gene, named *eca1*. The accession number for *eca1* is AJ577087.

Strains and Plasmids

All strains had the genetic background of FB1 (*a1b1*) or FB2 (*a2b2*; for details of plasmids and strains, see Table 1). In FB2Δ*Eca*1 *eca1* was deleted by a complete replacement with a phleomycin resistance cassette. For in vivo analysis of green fluorescent protein (GFP)-marked MTs, the a GFP-α-tubulin–encoding plasmid (potefGFPTub1; Table 1) was ectopically integrated into the succinate-dehydrogenase locus of strains FB1, FB2Δ*Eca*1, and FB1Dyn2^{ts}, resulting in FB1GT, FB1 and Dyn2^{ts}GT, and FB2GT and FB2ΔEca1GT, respectively. For localization of *U. maydis* GFP-myosin V plasmid, pOG-Myo5 was introduced in FB2ΔMyo5 (Weber *et al*., 2003) and FB2Δ*Eca*1. The ER network in FB2Δ*Eca*1 was visualized by integration of plasmid pERGFP (Wedlich-Söldner *et al*. 2002a), and colocalization studies were done in strain FB2EYEC that was derived from FB2 transformed with plasmids pEca1YFP and pERCFP. Strain FB2ΔEca1Dyn2^{ts} was generated by replacing *dyn2* by the temperature-sensitive allele *dyn2*^{ts}. In this strain, potef-GFP-Tub1 was introduced, resulting in FB2ΔEca1Dyn2^{ts}GT. For detection of intracellular calcium, a GFP-based Ca^{2+} probe (Nakai *et al*., 2001) was put under the control of the *otef*-promoter and ectopically integrated in FB2 and FB2Δ*Eca*1 cells. All integrations were confirmed by Southern blot analysis, and transformants were checked for proper morphology and doubling time to minimize possible defects due to the integration. For functional complementation of yeast strain K616 (Cunningham and Fink, 1994), *eca1* was expressed under the control of the *gal*$_{1-10}$-promoter (pGEca1, derived from plasmid YEplac195; kindly provided by Dr. H. Ulrich, MPI Marburg, Germany).

Growth Conditions

Strains were grown at 22 and 30°C in CM medium (Holliday, 1974) supplemented with 1% glucose (CM-G) or nitrate minimal medium supplemented

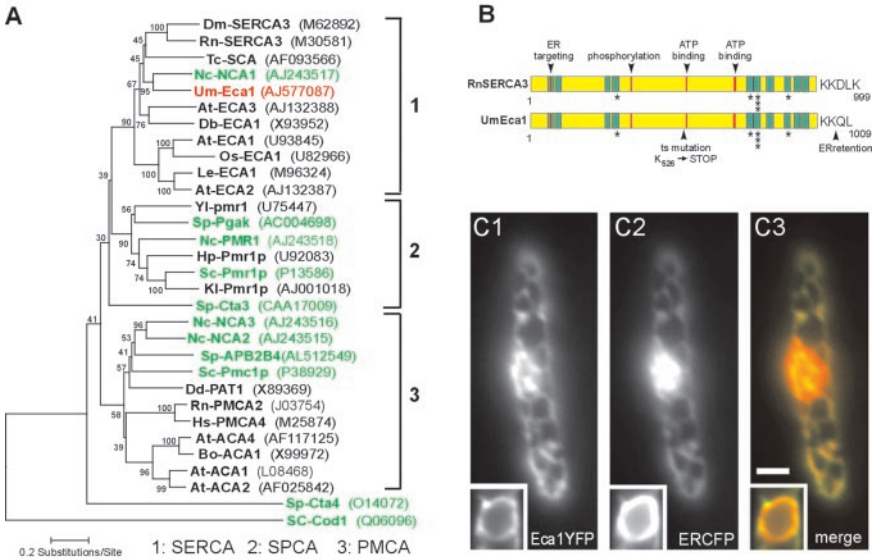

Figure 1. *Eca*1 belongs to type 3 SERCAs and localizes to the ER. (A) *Eca*1 groups with other sacroplasmic/ER Ca^{2+} ATPases (SERCA) in a dendrogram. Fungal Ca^{2+} ATPases are highlighted in green. SPCA, secretory pathway Ca^{2+}-ATPase; PMCA, plasma membrane Ca^{2+}-ATPase. Bootstrap values are at each node and accession numbers are in parentheses. (B) Domain organization of *Eca*1 and SERCA3 from rat. Predicted transmembrane domains are indicated in green, and residues involved in Ca^{2+} binding are marked with an asterisk. Note that the temperature-sensitive mutation in *Eca*1^{ts} results in a STOP codon. (C) An Eca1YFP fusion protein and an ER-targeted ER-CFP fusion protein (C2) colocalize within the peripheral ER network and the nuclear envelope (insets) of haploid *U. maydis* cells. Bar, 2 μm.

with 5.6 mM Ca^{2+} (NM; Holliday, 1974) and without Ca^{2+} (NM/low Ca^{2+}). Temperature shift experiments by using strains containing the *dyn2*^{ts}-allele were done as described previously (Wedlich-Söldner *et al*., 2002a). For temperature shifts of Δ*eca1* mutant strains, 20 ml of liquid cultures was grown overnight in CM-G at 22°C to $OD_{600} < 1$, and 3–5 ml of this culture was supplemented with dimethyl sulfoxide, benomyl, KN-92, or KN-93 (Calbiochem, San Diego, CA) and shifted to 30°C in a water bath. Salt conditions were analyzed at 22°C. For low Ca^{2+} experiments, cells of 15-ml overnight cultures were washed twice in 15 ml of precooled water and resuspended in 5 ml of NM or NM/low Ca^{2+} medium, followed by incubation for 4 h at 30°C in culture flasks that were rinsed with ultrapure water. Colony growth of K616 derivatives was monitored on synthetic complete medium without uracil supplemented with 10 mM $CaCl_2$ or 40 mM EGTA. Plate growth of *U. maydis* was analyzed on CM-G plates containing $CaCl_2$ (1–1000 mM), EGTA (1–500 mM), LiCl (1–1000 mM), and NaCl (1–1000 mM). Inhibitor effects were analyzed on CM-G plates supplemented with the solvent dimethyl sulfoxide or ethanol, 0.5–3 μM benomyl, 10 μM cytochalasin D, 1–20 μM taxol, 1–10 μM tunicamycin, 1.5–3 mM dithiothreitol (DTT), 15–30 μg/ml cyclosporin A, and 1–4 μg/ml FK506 (kindly donated by Fujisawa GmbH, Munich, Germany). Unless otherwise noted, chemicals were purchased at Sigma Chemicals.

Southern, Northern, and Western Analysis

DNA isolation from *U. maydis* and transformation procedures were carried out as described previously (Krüger *et al*., 1998). RNA was isolated from strains grown in liquid culture for 3 h and prepared as described previously (Krüger *et al*., 1998). A 2005-bp *Sac*II-*Kpn*I fragment of *eca1* was used as a probe. Western analysis was done as described previously (Straube *et al*., 2001) by using a monoclonal GFP antibody (Roche Diagnostics, Mannheim, Germany) and horseradish peroxidase-coupled anti-mouse IgG (Promega, Madison, WI).

Sequence Analysis

Phylogenetic dendograms were constructed using ClustalX and MEGA 2.1 (http://www.megasoftware.net) by using the minimum evolution or maximum parsimony algorithms and gap deletion option. Then 500 replicates were used for bootstrap support. Domain and motif analysis was carried out using BLAST (http://www.ncbi.nlm.nih.gov/blast/) and SMART (http://smart.embl-heidelberg.de) servers. Transmembrane helices were predicted with ISREC (http://www.ch.embnet.org). The genome of *U. maydis* was accessed at http://www.genome.wi.mit.edu/annotation/fungi/ustilago_maydis/index.html).

Light Microscopy and Image Processing

Microscopic analysis was performed using an Axioplan II microscope (Carl Zeiss, Jena, Germany). Frames were taken with a cooled charge-coupled device camera (C4742-95; Hamamatsu, Bridgewater, NJ). Epifluorescence of GFP was observed using the standard fluorescein isothiocyanate filter sets. Colocalization of YFP and CFP was analyzed with specific filter sets (YFP: BP500/20, FT515, and BP535/30; and CFP: BP436, FT455, and BP480-500). Quantification and image processing, including adjustment of brightness, contrast, and gamma values, was performed with ImageProPlus (Media Cybernetics, Gleichen, Germany), MetaMorph (Universal Imaging, Downingtown, PA), and Photoshop (Adobe Systems, Mountain View, CA).

Detection of Cytosolic Ca^{2+}

Cells expressing a GFP-based calcium probe (Nakai *et al*., 2001) were grown in CM-G at 22°C. Cells were shifted incubated for 3 h at 30°C in a water bath, and samples were observed at 50% of lamp intensity (Atto Arc; Carl Zeiss) by using the standard fluorescein isothiocyanate filters and a cooled charge-coupled device camera (Coolsnap HQ; Photometrics, Tucson, AZ). To minimize the risk of artifacts due to oxygen depletion or radiation, only two to three cells per preparation were observed without embedding in agarose. Average cytoplasmic signal intensities were measured and corrected by the background noise and the autofluorescence of FB2 cells by using MetaMorph (Universal Imaging).

Quantification of Morphology Defects, ER Motility, and Microtubule Dynamics

For microscopic observation, cells from logarithmic cultures were embedded in 1% low melt agarose. Unless stated, morphology of control and Δ*eca1* mutant cells was analyzed after 4–5 h at 30°C. Cell morphology was considered "abnormal" if cells were multiple budded, branched, or irregularly shaped. For each experiment, at least 100 cells were analyzed. ER motility and MT dynamics was measured as described previously (Steinberg *et al*., 2001; Wedlich-Söldner *et al*., 2002a). All analysis was done using digital sequences of 30–60 frames that were taken with an exposure time of 500-1000 ms per frame at 40–60% lamp intensity. Microscopic preparations were observed no longer than 15 min to prevent defects due to oxygen depletion. All measurements were done using ImageProPlus (Universal Imaging). Statistical analysis by two-tailed t test at $\alpha = 0.05$ was carried out using Prism (GraphPad Software Inc., San Diego, CA).

RESULTS

Eca1 Is Similar to Mammalian SERCAs and Localizes to the ER

In a genetic screen for temperature-sensitive mutants, we obtained 63 strains that grew normally at 22°C but were unable to form colonies at 34°C. By complementing one of these mutant strains (FB1Eca1^{ts}) with a genomic library, we identified an open reading frame of 3030 base pairs that fully restored growth at 34°C (our unpublished data). *eca1* (accession no. AJ577087) encodes a putative protein of 1009 amino acids that shares highest sequence identity with animal type 3 PIIA SERCAs (47–58%) and with a putative Ca^{2+}-transporter from *Neurospora crassa* (60%, NCA1; Benito *et al*., 2000; Figure 1A). The gene product *Eca*1 is predicted to contain 10 transmembrane domains and all motifs characteristic of P-

type ATPases, including those implied in nucleotide binding and phosphorylation (Evans and Williams, 1998), as well as the evolutionary conserved Ca^{2+} binding sites (Clarke *et al*., 1989; Figure 1B). In addition, *Eca*1 contains an N-terminal ER targeting pentapeptide motif found in SERCAs (Magyar and Varadi, 1990) and a canonical dilysine C-terminal ER retention motif (KKQL; Andersson *et al*., 1999). To verify the predicted localization of *Eca*1 in the ER, we expressed an *Eca*1-GFP fusion protein in the *eca1* mutant strain FB1Eca1^{ts}. The fusion protein rescued the growth defect of the mutant and localized to a peripheral network and the nuclear envelope, a characteristic distribution of the ER (our unpublished data). To confirm this notion, we then coexpressed in wild-type cells a fusion protein of *Eca*1 and yellow fluorescent protein (*Eca*1-YFP; Figure 1C1) and an ER-targeted cyan-fluorescent derivative (ER-CFP; Figure 1C2) that has been previously shown to localize to the ER in *U. maydis* (Wedlich-Söldner *et al*., 2002a). Both *Eca*1-YFP and ER-CFP colocalized in all areas (Figure 1C3), thereby confirming that *Eca*1 resides in the ER.

Eca1 Functions in Ca^{2+} Homeostasis

Sequencing of the mutated *eca1* allele in FB1Eca1^{ts}, revealed a single point mutation (A to T) at nucleotide +1576 that changed residue K526 to a stop codon, therefore making it likely that, regardless of temperature, only a nonfunctional *Eca*1 protein is expressed in this mutant. Consequently, we deleted the entire *eca1* open reading frame. At 30°C, which is close to the optimum temperature of *U. maydis*, growth of the resulting strain FB2Δ*Eca*1 was reduced (Figure 3A; wt, wild-type control; Δeca1, Δ*eca1* mutant) and cell morphology of mutants was heavily impaired (see below), whereas morphology and the ability to form colonies was restored at 22°C and abolished at 34°C (Figure 2A).

Because the localization and sequence of *Eca*1 indicated a role in Ca^{2+} transport into the ER, we compared intracellular Ca^{2+} levels in wild-type and Δ*eca1* cells by using a GFP-based Ca^{2+} probe that exhibits fluorescence upon binding to Ca^{2+} (Nakai *et al*., 2001). Western analysis showed that the reporter gene was expressed at similar levels in reference strain FB2CMP (Figure 3A) and Δ*eca1* mutant strain FB2ΔEca1CMP (Δeca1CMP). A quantitative analysis on the single cell level revealed a faint Ca^{2+} signal at 30°C in reference cells that was slightly decreased at 22°C (Figure 3B, not significantly different from 22°C, $p = 0.1146$; for example, see 3C1 and 3C2). In contrast, Ca^{2+} levels were strongly elevated in Δ*eca1* cells at 30°C and significantly decreased at 22°C (Figure 3B, 3C2, and 3C4; $p < 0.0001$), indicating that *Eca*1 is required to maintain normal cytosolic Ca^{2+} concentrations. In some cases, growth of Δ*eca1* mutants was not restored at 22°C, and this coincided with high Ca^{2+} levels, indicating that abnormal morphology and elevated Ca^{2+} levels are related (Figure 3B).

To confirm a role of *Eca*1 in Ca^{2+} transport, we complemented the yeast mutant strain K616 (Cunningham and Fink, 1994), an approach that was successfully used to confirm Ca^{2+} transport activity of SERCA pumps before (Sze *et al*., 2000). In this yeast mutant, two Ca^{2+} ATPases, Pmc1p and Pmr1p, are deleted, resulting in a requirement for external Ca^{2+} supplies. On plates supplemented with Ca^{2+} the mutant K616 transformed with empty vector (control; Figure 3D) or vector carrying the *U. maydis eca1* gene (pGEca1; Figure 3D) formed colonies. However, growth of the control strain was abolished on a medium depleted for Ca^{2+} (control, 40 mM EGTA; Figure 3D), whereas expression of *eca1* restored viability of K616 under these conditions (Figure 3D). *Eca*1-YFP expressed in K616 localized to the nuclear envelope and a peripheral network (arrow in Figure 3E), which suggests that *Eca*1 complements the defects of K616 by its Ca^{2+}-pumping activity at the ER.

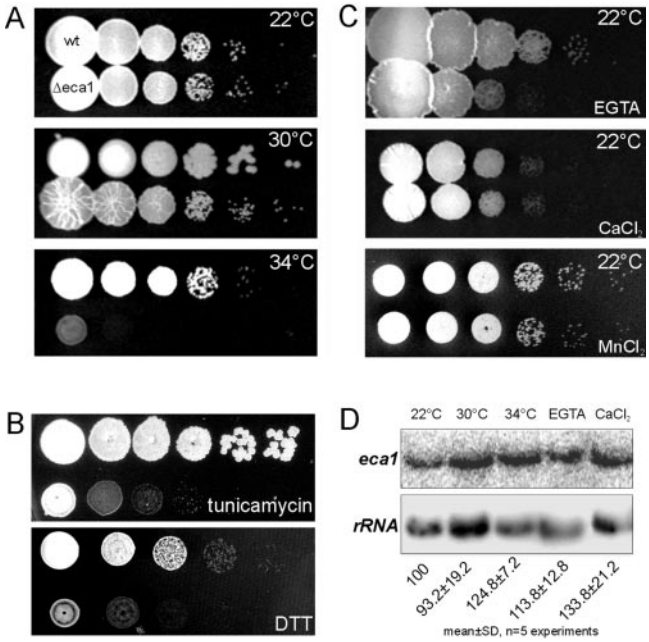

Figure 2. Δ*eca1* mutants are sensitive to temperature, EGTA, and ER stress. (A) Growth of wild-type control (wt) and Δ*eca1* mutants (Δeca1) at 22, 30, and 34°C. Note that regular growth temperature for *U. maydis* is 28–30°C. (B) Growth of wild-type and Δ*eca1* mutants at 22°C on plates containing tunicamycin (2.5 μg/ml) and DTT (2 mM). Both inhibitors affect protein processing within the ER, suggesting that Ca^{2+}-dependent protein folding in the ER is impaired in Δ*eca1* mutants. (C) Growth at 22°C on agar supplemented with EGTA (5 mM), Ca^{2+} (250 mM), or Mn^{2+} (10 mM). Note that treatment with $CaCl_2$ did not affect colony formation, but had a negative effect on cell morphology and MT organization (Figure 4, C and H). (D) Northern analysis of *eca1* expression in FB2 under temperature and Ca^{2+} stress conditions. The experiment was repeated five times and *eca1* signals at 22°C, corrected by loading controls, were normalized to 100%. Note a significant increase under 50 mM Ca^{2+} and 34°C.

Because these data argue for a role of *Eca*1 in Ca^{2+} transport into the ER, where Ca^{2+} ions are needed for ER-dependent folding of secretory proteins, we tested this ER function in Δ*eca1* cells. We generated ER stress by treatment with tunicamycin (2.5 μg/ml) and DTT (2 mM), which affect *N*-glycosylation and folding reactions in ER. Wild-type cells still grew under these conditions, but both agents inhibited growth of Δ*eca1* already at 22°C (Figure 2B). This hypersensitivity indicates that ER-based protein processing is compromised in Δ*eca1* mutants, which might be the cause of the lethal phenotype at 34°C. Growth of Δ*eca1* strains was also sensitive to EGTA (5 mM; Figure 2C), but neither high concentrations of Ca^{2+} (250 mM) nor Mn^{2+} (10 mM) inhibited colony formation, although most Δ*eca1* cells showed a pronounced morphology defect under these conditions (see below). Finally, Northern analysis indicated that *eca1* was expressed at similar levels under various stress conditions, and a slight increase was only found at high temperature ($p = 0.018$) or 50 mM extracellular Ca^{2+} ($p = 0.015$; Figure 2D). In summary, these data strongly indicate that *Eca*1 regulates Ca^{2+} homeostasis by pumping cytosolic Ca^{2+} into the ER.

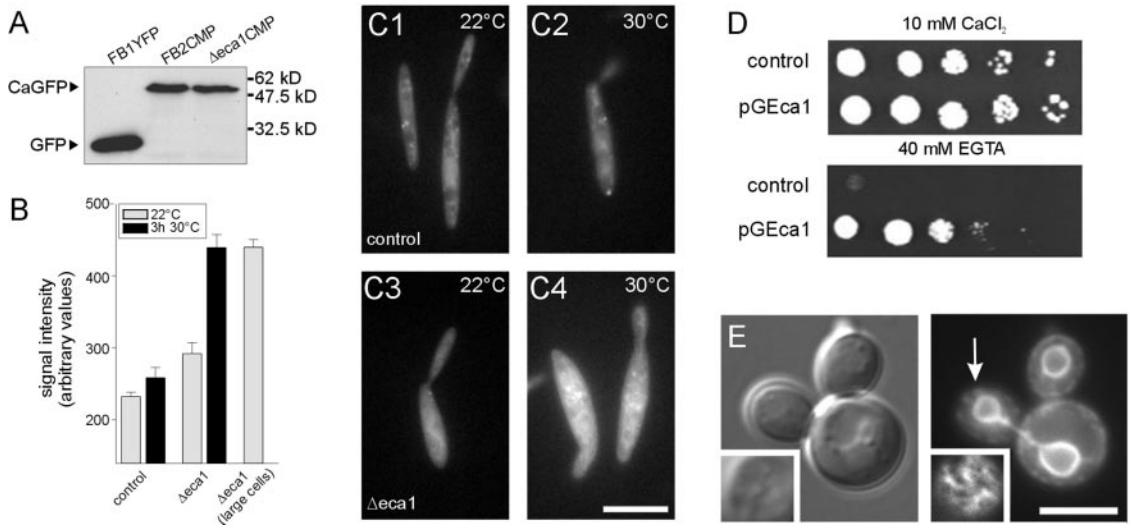

Figure 3. *Eca*1 functions in Ca^{2+} homeostasis. (A) Western blots of cell extracts of strains that express a cytoplasmic GFP-based Ca^{2+} probe (Nakai *et al*., 2001). An anti-GFP antibody detects the M13-cpEGFP-CaM fusion protein in reference strain FB2CMP and mutant strain FB2ΔEca1CMP. Detection of YFP in extracts of FB1YFP is given as control. (B) Quantitative analysis of Ca^{2+} sensitive M13-cpEGFP-CaM signals at 22 and 30°C. At 22°C, cells of reference strain FB2CMP show faint cytoplasmic staining that slightly increases after shift to 30°C. In contrast, in normal shaped Δ*eca1* mutants the M13-cpEGFP-CaM-based fluorescence is already slightly evaluated, and growth at 30°C significantly increased the signal. A small portion of Δ*eca1* mutant cells show impaired morphology at 22°C that coincides with increased M13-cpEGFP-CaM fluorescence. Note that the graph was corrected for the background signal of *U. maydis* cells without GFP. Sample size is 18–34 cells and 4 for "Δ*eca1* large cells" at 22°C. (C) Examples of M13-cpEGFP-CaM signals in cells of reference strain FB2CMP and mutant strain FB2ΔEca1CMP. Bar, 10 μM. (D) Yeast strain K616 expressing a control plasmid (control) is unable to grow in the absence of Ca^{2+}. Expression of *eca1* (pGEca1) complements this defect, demonstrating that *Eca*I is involved in Ca^{2+} homeostasis. (E) Differential interference contrast image and corresponding fluorescence image of yeast strain K616Eca1YFP that expresses a functional *Eca*1-YFP fusion protein. Note that *Eca*1 localizes to the ER and the nuclear envelope (white arrow, insets show peripheral focal plane). Bar, 2 μm.

Eca1 Is Required for Interphase MT Organization and Polar Growth

At 30°C, Δ*eca1* cells showed growth at both poles and formed multiple septa (Figure 4A2, 4 h at 30°C; septa indicated by arrows). This resulted in large cell aggregates with rounded and apolar cells (Figure 4A3, 12 h at 30°C). Under these conditions, wild-type cells were unaffected (Figure 4A3, inset, and 4C). Low temperature (22°C) restored morphology of Δ*eca1* cells (Figure 4A1, for wild-type control, see inset in Figure 4A3). Interestingly, this temperature phenotype was dependent on external Ca^{2+} concentration, because low extracellular Ca^{2+} suppressed the temperature-dependent Δ*eca1* phenotype (Figure 4B, compare with 4A2; 4C; 4 h at 30°C in NM with low Ca^{2+}). In addition, morphology of Δ*eca1* cells was more sensitive to high extracellular Ca^{2+} levels (250 mM; Figure 4C), which also affected the shape of wild-type cells but to a much smaller extent. Thus, *Eca*1 is required to maintain normal cell shape at 30°C and during Ca^{2+} stress.

Morphology of fungal cells is based on the cytoskeleton. Therefore, we speculated that the Ca^{2+}-dependent phenotype of FB2Δ*Eca*1 was due to defects in cytoskeletal organization or function. Therefore, we first monitored the effect of cytoskeleton inhibitors on plate growth of wild-type control and Δ*eca1*. In the presence of 10 μM of the actin inhibitor cytochalasin D, no difference between control and Δ*eca1* mutants was observed (Figure 4D), and this coincided with normal actin patch distribution in Δ*eca1* mutants at restrictive conditions (our unpublished data). Furthermore, in FB2Δ*eca1* transport along the actin cytoskeleton was apparently not impaired, because a functional GFP-myosin V fusion protein that requires F-actin for polar localization at the growth region (Weber *et al*., 2003) was correctly positioned at the cell poles (Figure 4E, 3 h 30°C). This suggested that elevated Ca^{2+} levels did not severely affect the actomyosin system. In contrast, Δ*eca1* mutant were more sensitive to the MT stabilizer taxol (5 μM) and less sensitive to low doses of destablizer benomyl (1 μM; Figure 4D). Moreover, 2.5 μM benomyl suppressed most of the temperature-dependent morphology defects of Δ*eca1* cells (Figure 4F1 and 4F2; 4 h at 30°C, compare with 4A2), indicating that growth and morphology defects of FB2Δ*eca1* are mainly due to unusually stable MTs. This notion was further supported by the observation that GFP-α tubulin-labeled MTs (Steinberg *et al*., 2001) in Δ*eca1* cells were much longer and irregular arranged (Figure 4G, Δeca1; see also 5D2) as in reference strain FB2GT (Figure 4G, control, 4 h at 30°C). Consistent with the restorative effect of lower temperature on morphology no obvious differences between the mutant and control cells were found at 22°C (Figure 4G). These results were confirmed by indirect immunofluorescence by using anti-tubulin antibodies in strains FB2 and FB2Δ*Eca*1, indicating that they are not due to expression of GFP-α tubulin (our unpublished data). Interestingly, disturbed MT patterns were observed in wild-type cells exposed to high extracellular Ca^{2+} (250 mM; Figure 4H), suggesting that aberrant MTs and cell shape are generally associated with increased Ca^{2+} levels. Together, these results argue for an effect of high cytosolic Ca^{2+} levels on morphogenesis by influencing MT stability in Δ*eca1*.

Ca^{2+} Signaling Is Involved in the Phenotype of Δeca1 Mutants

The effects of high Ca^{2+} levels on MTs might be mediated by effectors of Ca^{2+} signaling, Ca^{2+}/CaM dependent-kinases, and the phosphatase calcineurin. Similar to Δ*eca1*, cal-

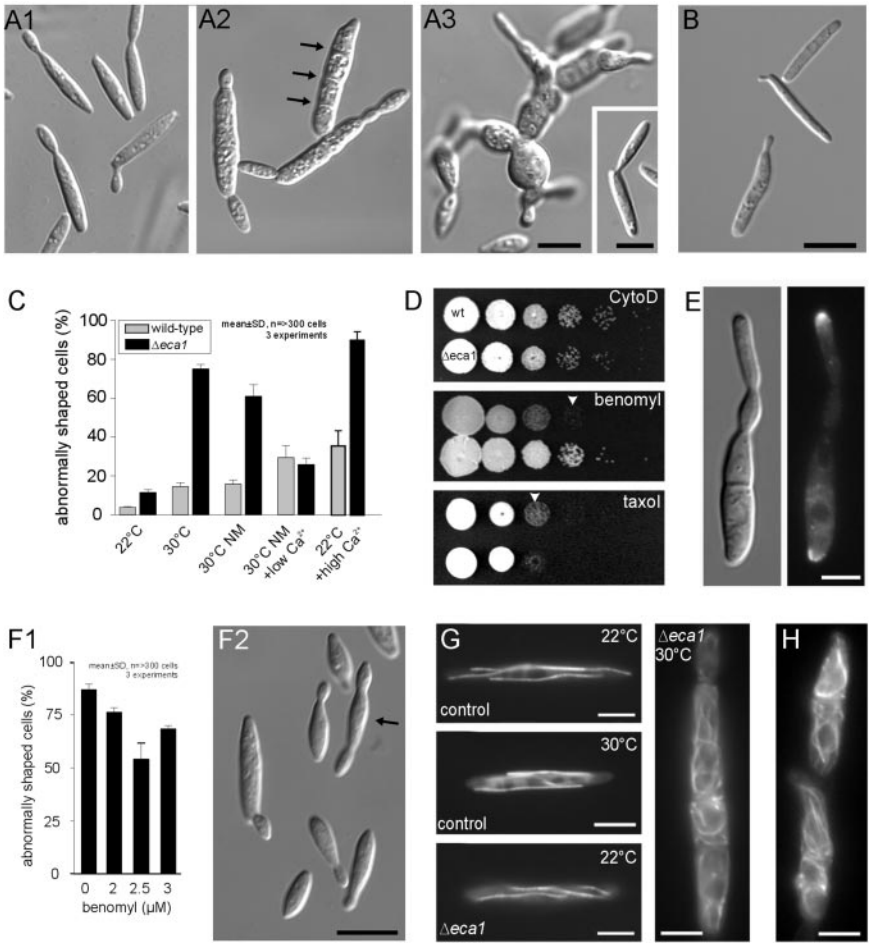

Figure 4. Temperature-dependent morphology defect of Δ*eca1* mutants is associated with defects in microtubule organization. (A) Morphology of Δ*eca1* mutant cells. At 22°C, Δ*eca1* mutant cells are similar to control cells (A1; for control, see inset in A3). At 30°C, cells enlarge, start to grow at both cell poles, and fail to separate (A2, septa indicated by arrows; 4 h at 30°C). With extended time at 30°C, Δ*eca1* mutant cells form large structures of unseparated and often rounded cells (A3, 12 h). Under the same conditions, the control strain FB2 is unaffected (A3, inset). Bars, 5 μm. (B) Morphology of Δ*eca1* mutant cells shifted in low Ca^{2+} medium. Reduction of external Ca^{2+} suppressed the morphology phenotype of Δ*eca1* cells after 4 h at 30°C. Bar, 5 μm. (C) Quantitative analysis of morphology defects of Δ*eca1* mutants compared with wild-type control. Morphology of strain FB2 was virtually unaffected by temperature, whereas 75–80% aberrant mutant cells were observed after 4–5 h at 30°C. Similar results were obtained in minimal medium supplemented with Ca^{2+} (NM). However, no difference between control and mutant cells was found in minimal medium with reduced Ca^{2+} (NM, low Ca^{2+}). *eca1* mutants are much more sensitive to treatment with 250 mM Ca^{2+}. All data points are based on three experiments with >100 cells each. For criteria of abnormal morphology, see MATERIALS AND METHODS. (D) Effect of cytoskeletal inhibitors on plate growth of wild-type and Δ*eca1* mutants strains. No difference between Δ*eca1* mutants and wild-type cells was found in the presence of the actin inhibitor cytochalasin D (10 μM). In contrast, Δ*eca1* cells are less sensitive to the MT destabilizing drug benomyl (1 μM, arrowhead) and slightly more sensitive to taxol (3 μM, arrowhead), indicating a link between MT stability and the growth phenotype of Δ*eca1* mutants. (E) Polar localization of a fusion of GFP and a class V myosin from *U. maydis* in Δ*eca1* mutants after 3h at 30°C. F-actin–dependent localization of GFP-Myo5 is not impaired in Δ*eca1*, suggesting that Myo5 transport activity is not impaired. Bar, 5 μm. (F) Effect of low concentrations of the microtubule inhibitor benomyl on morphology of Δ*eca1*. In liquid culture, 2.5 μM benomyl significantly restored morphology of Δ*eca1* (F1; 4–5 h at 30°C), with less cells showing separation defects or multiple budding. Note that even cells that were considered abnormal showed improved morphology (arrow in F2; for comparison, see 4A2 and 4E). Bar, 10 μm. (G) Organization of MTs in FB2GT and FB2 ΔEca1GT. At 22 and 30°C (4 h), control cells contained straight MTs, labeled with GFP-αtubulin. At 22°C, Δ*eca1* mutants contain normal MTs, but at 30°C MTs became longer and heavily disordered (4 h at 30°C). Note that MTs leave the focal plane, thereby looking shorter. Bar, 5 μm. (H) Reference strain FB2GT treated with high levels of Ca^{2+} (250 mM, 4 h). High external Ca^{2+} strongly affected MT organization in many cells, which is reminiscent of MT defects in Δ*eca1* mutants at 30°C and normal Ca^{2+} levels. Bar, 5 μm.

cineurin mutants in fungi show poor viability under ER stress conditions (Bonilla *et al*., 2002; Cruz *et al*., 2002). In addition, these mutants are sensitive to cations such as Li^{2+} and Na^{+}. Consequently, we checked plate growth of Δ*eca1* mutants on LiCl (7.5 mM) and NaCl (0.5 M). No growth inhibition was observed, and Δ*eca1* cells grew even slightly better on LiCl, indicating that calcineurin was not inhibited in these cells (Figure 5A). Moreover, exposure of Δ*eca1* mutants to the specific calcineurin inhibitors cyclosporin A (15 μg/ml) or FK506 (4 μg/ml; Ho *et al*., 1996), led to a significant reduction in growth at 30°C (Figure 5A), whereas wild-type cells were not affected. In other words, the dephosphorylation activity of calcineurin is crucial for survival of Δ*eca1* on plates.

In contrast, the inhibition of CaMK by the potent inhibitor KN-93 (Sumi *et al*., 1991) had a positive effect on Δ*eca1* cells. Treatment with 60 μM KN-93, but not with its inactive structural analogue KN-92, restored near-normal morphology to Δ*eca1* mutants at 30°C (Figure 5B1 and 5B2), whereas this treatment did not affect morphology of wild-type cells (Figure 5B3). Restoration of morphology by KN-93 treatment was accompanied by the formation of nearly normal interphase MT arrays (Figure 5C1) in ~70% of all cells after 3 h at 30°C, whereas MT arrays in KN-92–treated cells were disordered and resembled the characteristic Δ*eca1* phenotype (Figure 5C2). Thus, altered Ca^{2+}-homeostasis in Δ*eca1* mutants seems to increase CaMK activity, which in turn deregulates MT dynamics and results in morphology defects.

Δeca1 and Dynein Mutants Share Virtually Identical Alterations in Microtubule Dynamics

The defect in MT organization in FB2Δ*eca1* resembled that of dynein mutants (Straube *et al*., 2001). Therefore, we examined the relationship between *eca1* and dynein effects on MT dynamics. We first analyzed the role of dynein in MT organization by using a temperature-sensitive allele of the dynein heavy chain (*dyn2*^{ts}; Wedlich-Söldner *et al.* 2002a). At

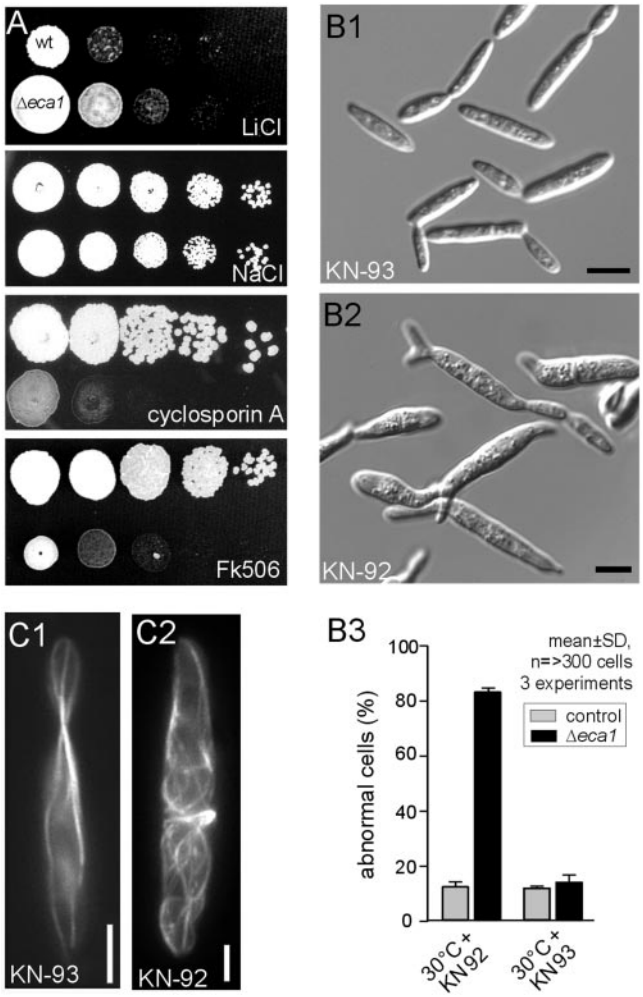

Figure 5. Δ*eca1* mutants require the Ca^{2+}-dependent phosphatase calcineurin for stress tolerance, and show increased CaMK activity. (A) Δ*eca1* mutants show normal growth at high levels of Li^{2+} (7.5 mM) and Na^{2+} (0.5M). Calcineurin inhibition with cyclosporin A (15 μg/ml) or FK506 (4 μg/ml), result in reduced viability of Δ*eca1* mutants at high temperature (30°C). This aggravation of the phenotype by inhibition of Ca^{2+}-dependent protein dephosphorylation suggests that protein phosphorylation is involved in the observed defects of Δ*eca1* cells. (B) Inhibition of CaMKs restored the morphology phenotype of Δ*eca1* mutants at 30°C. Δ*eca1* mutants showed normal morphology at 30°C when grown in the presence of the specific CaMK inhibitor KN-93 (60 μM; B1). In contrast, the inactive analogue KN-92 has no restorative effect (B2 and B3). This observation argues for an involvement of Ca^{2+}-dependent protein phosphorylation in the Δ*eca1* phenotype. Bars, 5 μm. (C) Inhibition of CaMKs rescues the MT defect of Δ*eca1* mutants at 30°C. In FB2ΔEca1GT, KN-93 (C1) restores organization of MTs, but the inactive analogue KN-92 was without effect (C2). Bars, 2 μm.

permissive temperature, MTs in *dyn2*^{ts} and control cells were indistinguishable (Figure 6, A and B, 22°C), but inactivation of dynein at 29–30°C led to much longer, curved, and disorganized MTs (Figure 6B, 4–6 h at 29°C). This phenotype was reminiscent of Δ*eca1* mutants (compare Figures 6B and 4H or 5C2). In both mutants, MTs seemed less dynamic and more often growing MTs were observed (Figure 6C, *dyn*^{ts}; 6D, Δ*eca1*).

MT length depends on the velocity of elongation and shrinkage, as well as the frequency by which MTs switch from growth to shrinkage (catastrophe) and vice versa (rescue; Verde *et al*., 1992). To gain deeper insight into the MT phenotype, we measured these parameters of dynamic instability in Δ*eca1* and *dyn2*^{ts} mutant strains and compared the results to their reference strains. In both mutants, the velocity of elongation and shrinkage of MTs was almost unaltered, but in Δ*eca1* and *dyn2*^{ts} cells rescue rate was threefold increased and catastrophe rates were twofold lowered (Figure 6E and Table 2). Thus, it seems that shrinking MTs more often restart growth, whereas elongating MTs less often switch to depolymerization, explaining the abnormally long MTs in *dyn2*^{ts} and Δ*eca1* mutants. Inhibition of CaMKs by KN-93 resulted in almost normal MT organization of Δ*eca1* at 30°C (see above), and MT elongation and shrinkage rates, as well as rescue frequencies of Δ*eca1* mutants were restored to near normal levels (Figure 6F and Table 2). In contrast, MT defects in dynein mutants were not restored by the CaMK inhibitor KN-93 (Figure 6B), indicating that KN-93 acts upstream of the dynein complex in regulation of MT stability.

Δeca1 Mutants Are Defective in Dynein-dependent ER Motility

To gain further support for the hypothesis that the defects of Δ*eca1* mutants are due to altered dynein activity, we examined the effect of deletion of *eca1* on another dynein-dependent process. The peripheral tubular ER network in *U. maydis* is highly dynamic (Figure 7A1, arrow; see inset for higher magnification) and this motility is solely dynein-dependent (Wedlich-Söldner *et al*., 2002a). To analyze ER organization and motility in Δ*eca1* cells, we generated a strain that expressed an ER-targeted GFP fusion protein (FB2ΔEca1EG). At 22°C, the ER was localized at the cell periphery of both Δ*eca1* and control cells (our unpublished data) and directed tubule motility in both strains was indistinguishable (Figure 7C; Δ*eca1*: 4.12 ± 0.36 events/h × μm^2; reference: 4.59 ± 0.60 events/h × μm^2, n > 35 cells from three experiments; p = 0.3288). Temperature shift had no effect on the ER in control cells, but under these conditions Δ*eca1* mutants contained an irregular network of ER tubules that were no longer located at the cell periphery (Figure 7, B and D). At elevated temperature, ER motility in control cells increased, but directed ER tubule motion in Δ*eca1* was significantly reduced (Figure 7, B and C; Δ*eca1*: 1.40 ± 0.14 events/h × μm^2, reference: 8.94 ± 0.23 events/h × μm^2; n = 3 experiments and >38 cells; p > 0.0001). This defect in ER-motility in Δ*eca1* corresponds well with that of dynein mutants (Figure 7C; not significantly different, p = 0.1340, values for *dyn2*^{ts} from Wedlich-Söldner *et al*., 2002a). To analyze minor effects on ER motility, we did a quantitative comparison of digital images at two time points by using the software package MetaMorph. Again, we measured significantly less total ER displacement in Δ*eca1* than in control cells (p = 0.0059; 10–13 measurements, 28 cells). Finally, we set out to rescue the ER motility defect by the CaMK inhibitor KN-93. Although this CaMK inhibitor had no effect on ER in control cells at 30°C, KN-93 treatment led to fragmentation and disorganization of the ER networks in Δ*eca1* mutants that did not allow a study of motility. Interestingly, temperature shift led to a nuclear distribution defect in Δ*eca1*. Control cells contained a single nucleus in the cell center that is detectable by ER-GFP in the nuclear envelope (Figure 7A, arrowhead). However, Δ*eca1* at 30°C often contained numerous nuclei (Figure 7D, overnight 30°C; see also arrow in Figure 7B) that were also detected by 4,6-diamidino-2-phenylindole staining of DNA (Figure 7E, arrowheads; maximum-Z-axis projection of cells grown overnight at 30°C).

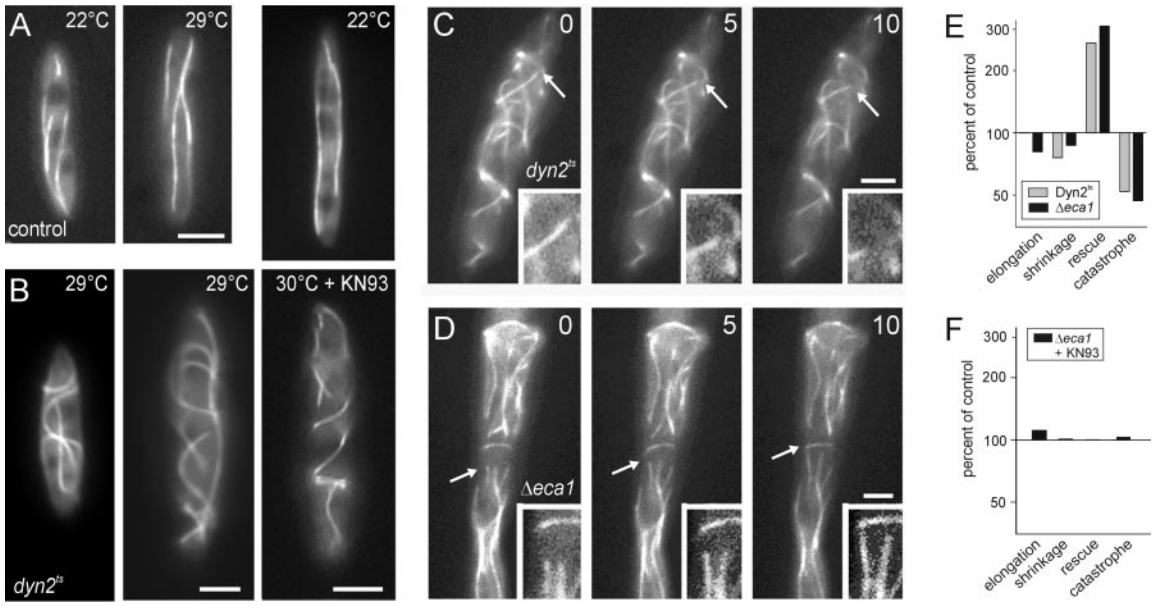

Figure 6. Conditional dynein mutants and Δ*eca1* mutants share defects in MT dynamics and organization. (A) Reference strain FB1GT contained straight GFP-labeled MTs at 22 and 29°C. Bar, 3 μm. (B) MTs were normal in dynein mutants that contain a temperature-sensitive dynein allele (Wedlich-Söldner *et al.* 2002a), but severely altered at restrictive conditions (4–6 h at 29°C). Treatment with the CaMK inhibitor KN-93 was without effect on the dynein phenotype at restrictive conditions (3.5 h at 30°C). Note that this phenotype resembles that of Δ*eca1* mutants. Bars, 3 μm. (C and D) Dynamic behavior of MTs in *dyn2*^{ts} (C) and Δ*eca1* (D) mutants. At restrictive temperature, both strains contain numerous curved MTs that show dynamic instability, including shrinkage due to depolymerization (arrow and inset in C) and polymerization-based elongation. Time in seconds is given in the upper right corner. Bar, 3 μm. (E) Parameters of MT dynamic instability in FB1Dyn2^{ts}GT and FB2ΔEca1GT at restrictive conditions compared with reference strains FB1GT and FB2GT, respectively. Note the striking similarity between Δ*eca1* and *dyn2*^{ts} mutants. For actual numbers, see Table 2. (F) CaMK inhibition by KN-93 restores most parameters of dynamic instability but did not affect the catastrophe value. Nevertheless, most mutant cells contained well-organized and shorter MTs.

Such a defect is characteristic of dynein mutants (Straube *et al*., 2001), again supporting the notion that dynein function is impaired in Δ*eca1*. Together, these results demonstrate that dynein-dependent motility of ER tubules is significantly impaired in Δ*eca1* mutants, again indicating that elevated Ca^{2+} levels in Δ*eca1* affect dynein activity.

Dynein and Eca1 Double Mutants Show Synthetic Growth Phenotypes, but No Increase in MT Defects

To gain deeper insights in the functional relationship between *Eca*1 and dynein, we generated strain FB2ΔEca1Dyn2^{ts}. Shifting this double mutant to 30°C simultaneously inactivated dynein and increased cytosolic Ca^{2+}. Assuming that *Eca*1 and dynein act in the same pathway, inactivation of both should not increase the phenotype of the individual mutants. Growing mutants at 30°C in liquid culture resulted in a more severe morphological defect of the double mutant (Figure 8A, 11 h). In addition, at semipermissive conditions (Figure 8B, 28°C) the double mutant was clearly more impaired in plate growth, whereas growth of all mutants was the same at permissive temperature (Figure 8B, 22°C). However, mutations in *eca1* and dynein showed no synthetic effect on MT organization (Figure

Table 2. Dynamics of GFP-labeled MTs in Dyn2^{ts} and Δ*eca1* mutants and reference strains

		Elongation[a]	Shrinkage[a]	Rescue[b]	Catastrophe[b]
FB1GT[c]	22°C	10.3 ± 2.5 (19)	38.1 ± 19.8 (75)	0.48	2.64
	29°C[c]	10.6 ± 2.3 (19)	39.3 ± 20.9 (79)	0.66	3.24
FB1Dyn2^{ts}GT[c]	22°C	10.2 ± 2.2 (20)	39.5 ± 19.1 (70)	0.42	2.94
	29°C[c]	10.6 ± 2.5 (24)	29.7 ± 13.7 (80)	1.80	1.68
FB2GT[c]	22°C	7.9 ± 2.7 (10)	31.5 ± 17.1 (83)	0.24	3.30
	30°C[c]	8.4 ± 2.4 (13)	34.7 ± 17.6 (40)	0.42	2.82
FB2ΔEca1GT[c]	22°C	5.7 ± 2.5 (10)	31.9 ± 16.9 (43)	0.30	3.60
	30°C[c]	6.8 ± 2.0 (17)	30.3 ± 16.6 (44)	1.38	1.32
FB2ΔEca1GT+KN93[c]	30°C[c]	9.1 ± 2.1 (20)	35.0 ± 12.6 (41)	0.42	2.95
FB2ΔEca1Dyn2^{ts}GT	30°C[c]	5.5 ± 21.4 (9)	37.7 ± 18.8 (22)	12.66	1.02

[a] Rates given as mean ± S.D. (n) in micrometers per minute.

[b] Transitions per minute.

[c] Growth at 22°C, followed by 4–5 h of growth at 29°C or 30°C.

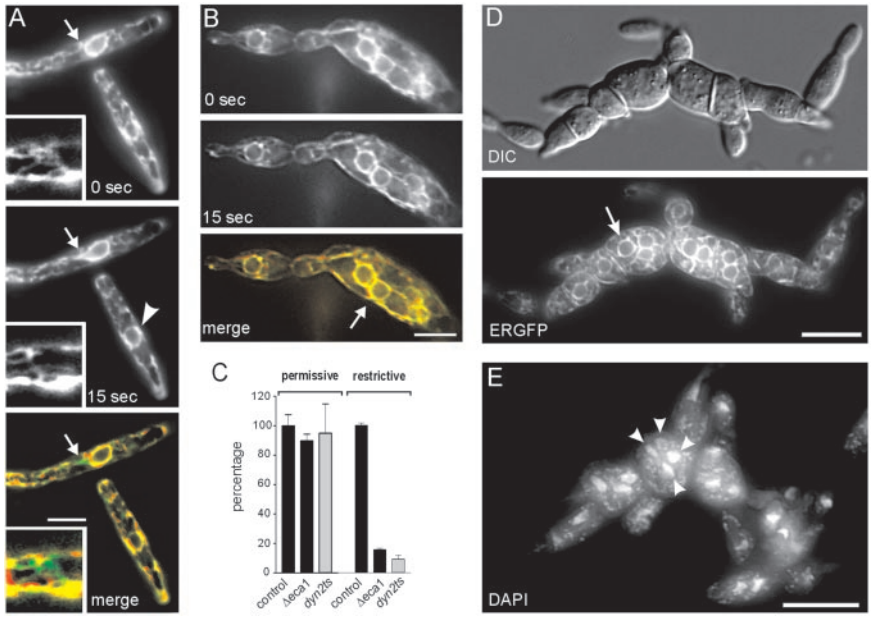

Figure 7. ER organization, ER motility, and nuclear migration in Δ*eca1* and dynein mutants. (A) ER motility in control cells. The network undergoes prominent motility (arrows; see inset for example at higher magnification) that is based on dynein activity (Wedlich-Söldner *et al*., 2002a). In pseudocolored overlay displacements reduce the regions of colocalization that are indicated in yellow. Arrowhead indicates the nuclear envelope. Time interval is given at the bottom. Bar, 5 μm. (B) ER motility in Δ*eca1*. There is significantly reduced ER tubule motility over the 15-s observation period, as can be seen from the pseudocolor merge image. Note that Δ*eca1* mutants contain an irregular network of ER tubules. This organization is in contrast to reference strain FB2EG, in which the ER network is localized to the cell periphery. Arrow indicates a nuclear envelope. Time interval is given at the bottom. Bar, 5 μm. (C) Quantitative analysis of ER motility in control, Δ*eca1* and dyn^{ts} cells. ER motility in Δ*eca1* mutants was measured as displacements per square micrometer and second according to Wedlich-Söldner *et al.* (2002a). Values for $dyn2^{ts}$ mutants are taken from the same reference. In both mutants ER motility is abolished at restrictive conditions. (D) Nuclear distribution defect in Δ*eca1* after overnight incubation at 30°C. Mutant cell form swollen cell chains that contained numerous nuclei, as indicated in corresponding fluorescent image of ER-GFP labeled nuclear envelopes (arrow). Bar, 10 μm. (E) DAPI staining of nuclei and fragmented mitochondria in Δ*eca1* at 30°C. Staining the nuclear DNA by DAPI (in one cell indicated by arrowheads) confirms the nuclear distribution defect of Δ*eca1.* Bar, 10 μm.

8C), and the alterations in MT dynamics in the double mutant were comparable with that of the Δ*eca1* single mutant strain (Figure 8D; changes in parameters compared with strain FB2ΔEca1GT). Therefore, we conclude that *Eca*1 and dynein are in the same pathway to regulate MT stability, which further supports the notion, an effect of Ca^{2+} signaling on MTs via the dynein complex. However, the increased growth defects of the double mutant argue for additional targets of Ca^{2+} signaling in morphology and cell separation.

DISCUSSION

Eca1 Is a Fungal SERCA-type Ca^{2+} Pump

In a screen for morphology mutants, we identified *eca1*, a putative Ca^{2+} transporter that shares highest sequence identity with SERCA-type pumps from animals and plants. This sequence similarity, the presence of conserved Ca^{2+} binding motifs, phosphorylation and ATP binding sites, and the overall domain structure argue for *Eca*1 being a true SERCA-type pump. Moreover, the localization of *Eca*1 in the ER and the functional complementation of the yeast mutant K616 that is impaired in Ca^{2+} homeostasis (Cunningham and Fink, 1994), and elevated levels of cytosolic calcium in Δ*eca1* mutants implicate a function for *Eca*1 in Ca^{2+} transport into the ER. However, Δ*eca1* cells grow almost normally at 22°C, suggesting that other Ca^{2+} pumps partially compensate for the loss of *Eca*1 at this temperature. In addition to the vacuolar and Golgi-localized Ca^{2+}-ATPases PMC1 and PMR1 in budding yeast (Cunningham and Fink, 1996), both budding and fission yeasts contain the V-subtype of ER-resident P-ATPases (Cronin *et al*., 2002; Facanha *et al*., 2002), which are also implicated in Ca^{2+} homeostasis. Surveys of the *Ustilago* genome (see MATERIALS AND METHODS) indicate that an orthologue of these proteins exists (47.7% identity and 64% similarity >1244 amino acids to Cta4p from *Schizosaccharomyces pombe*). Elucidating the role of this additional putative Ca^{2+} pump and their functional interplay with *Eca*1 will be a challenge for the nearer future.

Deregulated Ca^{2+} Signaling Is Responsible for the Defect of Δeca1 Mutants

*Eca*1 is dispensable at low temperature but is required to maintain morphology at 30°C. This indicates that a rise in temperature creates conditions under which transport of Ca^{2+} into the ER becomes crucial for the cell. In addition, treatment with tunicamycin and DTT, which targets protein modification and folding in the ER (Bonilla *et al*., 2002), is lethal to Δ*eca1* cells. A likely explanation for these observations is that higher temperatures increase the need for Ca^{2+}-dependent protein folding in the ER and that *Eca*1 activity is required to provide Ca^{2+} as a cofactor for ER-resident chaperones (Corbett and Michalak, 2000). Obviously, this raises the possibility that misfolding of secretory proteins in the ER cause the observed morphology defect. However, the morphology phenotype of Δ*eca1* can be suppressed by lowering extracellular Ca^{2+} and by specific inhibition of cytosolic CaMK by using KN-93 (Sumi *et al*., 1991). Moreover, in Δ*eca1* cytosolic Ca^{2+} is increased. This implies that temperature rise induces influx of extracellular Ca^{2+} that cannot be stored in the ER in the absence of *Eca*1. In this model, this transport defect elevates cytosolic Ca^{2+} levels and leads to an increase of CaMK activity (Figure 9). The high sensitivity of Δ*eca1* mutants to inhibition of calcineurin further supports this notion, because it indicates that this Ca^{2+}-dependent phosphatase counteracts the hyperactive CaMKs, thereby enabling Δ*eca1* to survive at 30°C. A link between calcineurin and CaMK-dependent signaling and cell morphology was also reported in fission yeast (Yoshida *et al*., 1994; Rasmussen, 2000) and in neurons (Chang *et al*., 1995). The accumulation of misfolded proteins in the ER of higher eukaryotes induces an entry of external Ca^{2+}

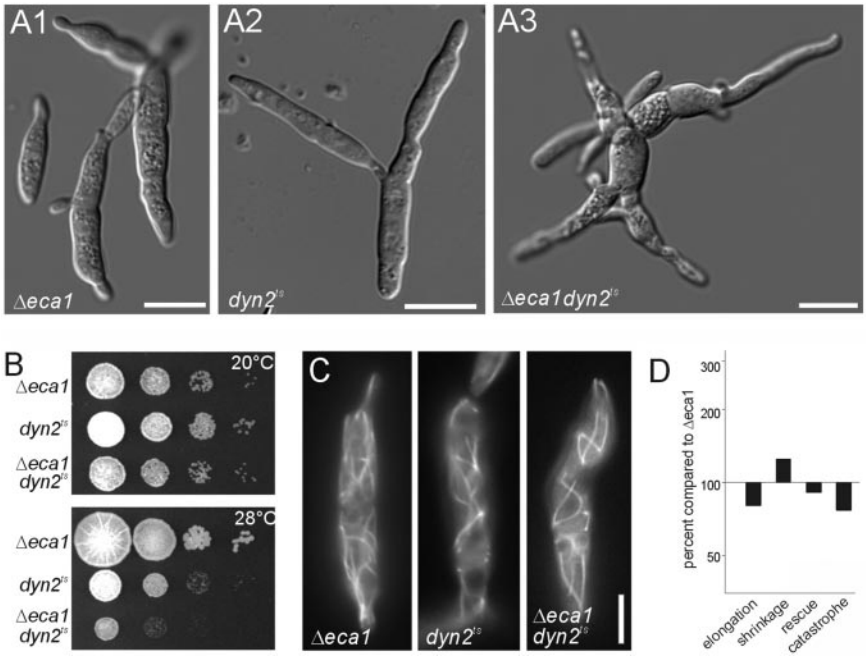

Figure 8. Analysis of a *eca1* and dynein double mutant. (A) Morphology of Δ*eca1*, *dyn*^{ts}, and a Δ*eca1 dyn*^{ts} double mutant. At 30°C, Δ*eca1* cells grow irregular, branch, and display defects in cell separation, which results in cell chains (A1). At the restrictive temperature (30°C), *dyn*^{ts} cells also show abnormal morphology, but cells tend to be longer and no cytokinesis defect was observed (A2). Under the same conditions, the double mutant showed an even stronger defect in cell shape (A3). Note that the morphology phenotype of the double mutant was very variable, ranging from branched cell chains to cells with long extensions. Bar, 10 μm. (B) Growth of Δ*eca1*, *dyn*^{ts}, and Δ*eca1 dyn*^{ts} mutants on agar plates. At permissive temperature (20°C), colony grow of all mutant strains was indistinguishable. However, at a semipermissive temperature (28°C), Δ*eca1* cells grow normal, whereas *dyn*^{ts} mutants show impaired colony formation. Interestingly, these conditions are almost lethal for the Δ*eca1 dyn*^{ts} double mutant. This additive phenotype indicates that Δ*eca1* and dynein mutants are defective in different cellular processes and mutations in both confer synthetic lethality at restrictive temperature. (C) Microtubules in Δ*eca1*, *dyn*^{ts}, and Δ*eca1 dyn*^{ts} mutants. All mutant strains contained longer and irregular organized microtubules. Bar, 5 μm. (D) Parameters of MT dynamic instability in FB2ΔEca1Dyn2^{ts}GT at restrictive conditions compared with the single mutant strain FB2ΔEca1GT (Δ*eca1*, black bars). Note that rescue rates of the double mutant resemble that of the Δ*eca1* single mutant and only slight effects on catastrophe values, shrinkage, and growth velocities were found. These data demonstrate that inactivation of dynein does not increase the effect of Δ*eca1* on MTs, which argues for a role of *Eca*I and dynein in the same pathway to regulate microtubule dynamics. For measured numbers, see Table 2.

into the cell (Putney *et al*., 2001), and SERCA activity is required to shuffle this Ca^{2+} into the ER (East, 2000). Therefore, we consider it most likely that similar mechanisms exist in *U. maydis* and that *Eca*1 is a key component facilitating survival and proper morphology under certain stress conditions.

Morphology Defects of Δeca1 Cells Are Due to Disordered MTs

Fungal growth and morphology depend on transport along the cytoskeleton, and a growing body of evidence indicates that MTs play a key role in this (Seiler *et al*., 1997; Sawin and Nurse, 1998; Wedlich-Söldner *et al*., 2000). Δ*eca1* mutants show severe defects in polar growth and cytokinesis, suggesting that cytoskeleton-based growth processes are affected. In agreement, the abnormal Δ*eca1* cells contained much longer and disorganized MTs, a defect that might be a consequence of deregulated dynamic instability of MTs. On the other hand, it is important to consider that elevated Ca^{2+} levels almost certainly affect numerous other cytoskeletal targets. For example, Myo5, a class V myosin involved in polar growth in *U. maydis* (Weber *et al*., 2003) contains a PEST site for Ca^{2+}-regulated proteolysis and a putative CaMK phosphorylation site that is implied in Ca^{2+}-dependent regulation of organelle traffic (Karcher *et al*., 2001). A functional GFP-myosinV fusion protein localized to the growing ends of Δ*eca1* cells, suggesting that Myo5 is not degraded and migrates along F-actin toward growth sites. Moreover, actin patch distribution was normal in Δ*eca1* (our unpublished data), indicating that the actin cytoskeleton is not severely affected by the deletion of *eca1*. On the other hand, high Ca^{2+} could interfere with other myosins or affect binding of Myo5 to secretory vesicles, thereby resulting in growth defects in Δ*eca1*. However, the Δ*eca1* growth and morphology defect was significantly restored by benomyl, which is thought to destabilize MTs at low concentrations (Willins *et al*., 1995). Thus, altered morphology of Δ*eca1* cells is most likely a consequence of altered MT dynamics, although it cannot be excluded that additional but so far undetected defects add to the observed phenotype.

Is Dynein a Target of Ca^{2+} Signaling to Regulate MT Length and Organization?

MT-associated proteins control dynamic instability (Walczak, 2000), and these components are potential targets of CaMKs (Gardin *et al*., 1997). Evidence exists for a role of dynein in the control of MT dynamics in fungi (Carminati and Stearns, 1997; Han *et al*., 2001), and our data presented here support a role of dynein in modifying MT stability. Surprisingly, both dynein and Δ*eca1* mutants show strikingly similar defects in MT dynamics. In both strains, MTs were longer, curved, and this is accompanied by a threefold increase in rescue rates and a twofold decrease in the frequency of MT catastrophe events. It is important to note that the altered parameters in MT number and dynamics are specific signatures for the dynein phenotype, because mutants in other MT-associated proteins or motors have different effects on MT dynamics (Walczak, 2000; our unpublished data). Therefore, the striking similarity between both the Δ*eca1* and dynein mutant phenotype is remarkable and, together with the restorative effect of CaMK inhibition on MT organization, suggest a link between Ca^{2+} signaling and dynein activity. In addition, the inactivation of dynein in Δ*eca1* mutants (strain FB2Deca1Dyn2^{ts}GT) did not significantly increase the defects in MT dynamics. In other words, MT defects in both Δ*eca1* and *dyn2*^{ts} background do not add in the double mutant, which supports our model of *Eca*1 acting on MT stability via dynein (Figure 9). This notion is further supported by the analysis of ER motility, a process that solely depends on cytoplasmic dynein in *U. maydis*

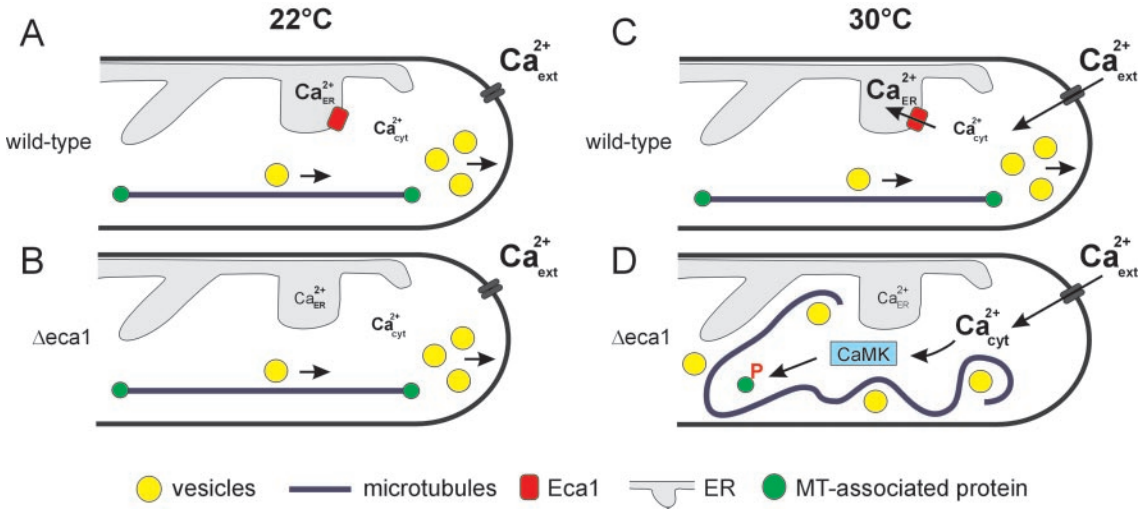

Figure 9. Model for the role of *Eca*1 in microtubule organization in *U. maydis*. (A) In wild-type cells, *Eca*1 is an ER-resident Ca^{2+} pump that maintains Ca^{2+} in the ER high and holds cytosolic Ca^{2+} below a toxic threshold ($Ca^{2+}{}_{cyt}$). MTs run along the axis of the cell to support directed MT-dependent delivery of supplies to the growth region. A fine-tuning of parameters of dynamic instability, including elongation and shrinkage velocities and catastrophe and rescue frequencies, controls most likely MT-length. (B) At 22°C, Δ*eca1* mutants display normal MTs and morphology suggesting that other Ca^{2+} pumps, such as a Cta4-like ATPse (for sake of clarity, not included) are sufficient to keep cytosolic Ca^{2+} levels low. However, the high sensitivity of Δ*eca1* mutants to ER stress suggests that $[Ca^{2+}]_{ER}$ is at a lower limit. (C) Increased temperature results in protein misfolding in the ER, which activates Ca^{2+}-dependent chaperones. This might induce store-mediated entry of extracellular Ca^{2+} through unknown channels, and *Eca*1 is required to pump this incoming Ca^{2+} into the ER, thereby maintaining $[Ca^{2+}]_{cyt}$ at resting levels. (D) In the absence of *Eca*1, incoming Ca^{2+} cannot be stored away, thus cytosolic Ca^{2+} increases, which activates CaMKs. These kinases phosphorylate MT-associated factors that regulate MT organization by influencing MT dynamic instability. A potential target of CaMK is cytoplasmic dynein that regulates MT dynamic instability and supports MT-dependent motility. These alterations in dynein activity and MT organization lead to defects in polar secretion and abnormal morphogenesis. Note that this model is supported by several key observations: 1) lowering external Ca^{2+} prevents the *ts*-phenotype of Δ*eca1*, 2) inhibition of CaMK restores MT-rescue values and leads to normal MT organization and morphology, and 3) artificially induced destabilization of MTs by benomyl treatment leads to significant reduction in morphology defects.

(Wedlich-Söldner *et al*., 2002a). In both Δ*eca1* and *dyn2*^{ts} mutants, ER tubule motility was inhibited to the same extent, whereas ER motility was not affected by disruption of F-actin or deletion of kinesin (Wedlich-Söldner *et al*. 2002a). Therefore, dynein activity is apparently impaired in Δ*eca1* mutants, and this might be a result of CaMK-dependent phosphorylation. Consistent with this hypothesis, it was recently shown that dynein activity in flagellar axonemes is modulated by CaMKs (Smith, 2002). Although *Ustilago* dynein heavy chain contains several potential CaMK phosphorylation sites, we consider it unlikely that the heavy chain is directly regulated by CaMKs. A good candidate for this regulation is the conserved 8-kDa dynein light chain that associates with calmodulin (Yang *et al*., 2001). However, details of the composition of the dynein complex in *U. maydis* are presently lacking.

In summary, our data are consistent with the notion that deletion of *eca1* that encodes a SERCA leads to deregulated Ca^{2+}-dependent signaling, which in turn affects MT dynamics via impaired dynein activity in *U. maydis*. SERCA activity is indispensable for Notch receptor and secretory protein transport in *Drosophila melanogaster* (Periz and Fortini, 1999), and defects in calcium homeostasis affect MT catastrophe rates and growth of fission yeast (Facanha *et al*., 2002). Therefore, the described link between Ca^{2+} signaling and MT-dependent exocytosis might be of general importance for eukaryotic cells.

ACKNOWLEDGMENTS

We are grateful to Dr. R. Kahmann for comments on the manuscript, Dr. K. Cunningham for strain K616, and Dr. H. Ulrich for yeast plasmids. We acknowledge Drs. J. Nakai and K. Imoto for providing the M13-cpEGFP-CaM construct, and Fujisawa USA Inc. for the gift of FK506. This work was supported by a grants from the Deutsche Forschungsgemeinschaft to G.S. (SP1111, STE799/4-1).

REFERENCES

Andersson, H., Kappeler, F., and Hauri, H.P. (1999). Protein targeting to endoplasmic reticulum by dilysine signals involves direct retention in addition to retrieval. J. Biol. Chem. *274*, 15080–15084.

Bannuett, F., and Herskowitz, I. (1989). Different a alleles of *Ustilago maydis* are necessary for maintenance of filamentous growth but not for meiosis. Proc. Natl. Acad. Sci. USA *86*, 5878–5882.

Benito, B., Garciadeblas, B., and Rodriguez-Navarro, A. (2000). Molecular cloning of the calcium and sodium ATPases in *Neurospora crassa*. Mol. Microbiol. *35*, 1079–1088.

Bölker, M. (2001). *Ustilago maydis* - a valuable model system for the study of fungal dimorphism and virulence. Microbiology *147*, 1395–1401.

Bonilla, M., Nastase, K.K., and Cunningham, K.W. (2002). Essential role of calcineurin in response to endoplasmic reticulum stress. EMBO J. *21*, 2343–2353.

Carminati, J.L., and Stearns, T. (1997). Microtubules orient the mitotic spindle in yeast through dynein-dependent interactions with the cell cortex. J. Cell Biol. *138*, 629–641.

Chang, H.Y., Takei, K., Sydor, L.A., Born, T., Rusnak, F., and Jay, D.G. (1995). Asymmetric retraction of growth cone filopodia following focal inactivation of calcineurin. Nature *376*, 686–690.

Clarke, D.M., Loo, T.W., Inesi, G., and MacLennan, D.H. (1989). Location of high affinity Ca^{2+}-binding sites within the predicted transmembrane domain of the sarcoplasmic reticulum Ca^{2+}-ATPase. Nature *339*, 476–478.

Corbett, E.F., and Michalak, M. (2000). Calcium, a signalling molecule in the endoplasmic reticulum? Trends Biochem. Sci. *25*, 307–311.

Cronin, S.R., Rao, R., and Hampton, R.Y. (2002). Cod1p/Spf1p is a P-type ATPase involved in ER function and Ca^{2+} homeostasis. J. Cell Biol. *157*, 1017–1028.

Cruz, M.C., Goldstein, A.L., Blankenship, J.R., Del Poeta, M., Davis, D., Cardenas, M.E., Perfect, J.R., McCusker, J.H., and Heitman, J. (2002). Calcineurin is essential for survival during membrane stress in *Candida albicans*. EMBO J. *21*, 546–559.

Cunningham, K.W., and Fink, G.R. (1994). Calcineurin-dependent growth control in *Saccharomyces cerevisiae* mutants lacking PMC1, a homolog of plasma membrane Ca^{2+} ATPases. J. Cell Biol. *124*, 351–363.

Cunningham, K.W., and Fink, G.R. (1996). Calcineurin inhibits VCX1-dependent H^+/Ca^{2+} exchange and induces Ca^{2+} ATPases in *Saccharomyces cerevisiae*. Mol. Cell. Biol. *16*, 2226–2237.

East, J.M. (2000). Sarco(endo)plasmic reticulum calcium pumps: recent advances in our understanding of structure/function and biology. Mol. Membr. Biol. *17*, 189–200.

Evans, D.E., and Williams, L.E. (1998). P-type calcium ATPases in higher plants - biochemical, molecular and functional properties. Biochim. Biophys. Acta *1376*, 1–25.

Facanha, A.L., Appelgren, H., Tabish, M., Okorokov, L., and Ekwall, K. (2002). The endoplasmic reticulum cation P-type ATPase Cta4p is required for control of cell shape and microtubule dynamics. J. Cell Biol. *157*, 1029–1039.

Fox, D.S., and J. Heitman. (2002) Good fungi gone bad: the corruption of calcineurin. Bioessays *24*, 894–903.

Gardin, H.M., Marklund, U., Larsson, N., Chatila, T.A., and Gullberg, M. (1997). Regulation of microtubule dynamics by Ca2+/Calmodulin-dependent kinase IV/Gr-dependent phosphorylation of oncoprotein 18. Mol. Cell. Biol., *17*, 3459–3467.

Gomez, T.M., and Spitzer, N.C. (1999). In vivo regulation of axon extension and pathfinding by growth-cone calcium transients. Nature *397*, 350–355.

Han, G., Liu, B., Zhang, J., Zuo, W., Morris, N.R., and Xiang, X. (2001). The *Aspergillus* cytoplasmic dynein heavy chain and NUDF localize to microtubule ends and affect microtubule dynamics. Curr. Biol. *11*, 719–724.

Hirokawa, N. (1998). Kinesin and dynein superfamily proteins and the mechanism of organelle transport. Science *279*, 519–526.

Ho, S., Clipstone, N., Timmermann, L., Northrop, J., Graef, I., Fiorentino, D., Nourse, J., and Crabtree, G.R. (1996). The mechanism of action of cyclosporin A and FK506. Clin. Immunol. Immunopathol. *80*, S40–S45.

Holliday, R. (1974). *Ustilago maydis*. In: Handbook of Genetics, ed. R.C. King, New YorK: Plenum Press.

Joseph, J.D., and Means, A.R. (2000). Identification and characterization of two Ca^{2+}/CaM-dependent protein kinases required for normal nuclear division in *Aspergillus nidulans*. J. Biol. Chem. *275*, 38230–38238.

Karcher, R.L., Roland, J.T., Zappacosta, F., Huddleston, M.J., Annan, R.S., Carr, S.A., and Gelfand, V.I. (2001). Cell cycle regulation of myosin-V by calcium/calmodulin-dependent protein kinase II. Science *293*, 1317–1320.

Kojic, M., Kostrub, C.F., Buchman, A.R., and Holloman, W.K. (2002). BRCA2 homolog required for proficiency in DNA repair, recombination, and genome stability in *Ustilago maydis*. Mol. Cell *10*, 683–691.

Krüger, J., Loubradou, G., Regenfelder, E., Hartmann, A., and Kahmann, R. (1998). Crosstalk between cAMP and pheromone signalling pathways in *Ustilago maydis*. Mol. Gen. Genet. *260*, 193–198.

Lehmler, C., Steinberg, G., Snetselaar, K.M., Schliwa, M., Kahmann, R., and Bolker, M. (1997). Identification of a motor protein required for filamentous growth in *Ustilago maydis*. Embo J. *16*, 3464–3473.

Magyar, A., and Varadi, A. (1990). Molecular cloning and chromosomal localization of a sarco/endoplasmic reticulum-type $Ca^{2(+)}$-ATPase of *Drosophila melanogaster*. Biochem. Biophys. Res. Commun. *173*, 872–877.

Nakai, J., Ohkura, M., and Imoto, K. (2001). A high signal-to-noise Ca(2+. probe composed of a single green fluorescent protein. Nat. Biotechnol. *19*, 137–141.

Periz, G., and Fortini, M.E. (1999). Ca^{2+}-ATPase function is required for intracellular trafficking of the Notch receptor in *Drosophila*. EMBO J. *18*, 5983–5993.

Putney, J.W., Jr., Broad, L.M., Braun, F.J., Lievremont, J.P., and Bird, G.S. (2001). Mechanisms of capacitative calcium entry. J. Cell Sci. *114*, 2223–2229.

Rasmussen, C.D. (2000). Cloning of a calmodulin kinase I homologue from *Schizosaccharomyces pombe*. J. Biol. Chem. *275*, 685–690.

Sawin, K.E., and Nurse, P. (1998). Regulation of cell polarity by microtubules in fission yeast. J. Cell Biol. *142*, 457–471.

Sebghati, T.S., Engle, J.T., and Goldman, W.E. (2000). Intracellular parasitism by *Histoplasma capsulatum*: fungal virulence and calcium dependence. Science *290*, 1368–1372.

Seiler, S., Nargang, F.E., Steinberg, G., and Schliwa, M. (1997). Kinesin is essential for cell morphogenesis and polarized secretion in *Neurospora crassa*. EMBO J. *16*, 3025–3034.

Smith, E.F. (2002). Regulation of flagellar dynein by calcium and a role for an axonemal calmodulin and calmodulin-dependent kinase. Mol. Biol. Cell. *13*, 3303–3313.

Steinberg, G., Wedlich-Soldner, R., Brill, M., and Schulz, I. (2001). Microtubules in the fungal pathogen *Ustilago maydis* are highly dynamic and determine cell polarity. J. Cell Sci. *114*, 609–622.

Straube, A., Brill, M., Oakley, B.R., Horio, T., and Steinberg, G. (2003). Microtubule organization requires cell cycle dependent nucleation at dispersed cytoplasmic sites, polar and perinuclear MTOCs in the plant pathogen *Ustilago maydis*. Mol. Biol. Cell *14*, 642–657.

Straube, A., Enard, W., Berner, A., Wedlich-Soldner, R., Kahmann, R., and Steinberg, G. (2001). A split motor domain in a cytoplasmic dynein. EMBO J. *20*, 5091–5100.

Stull, J.T. (2001). Ca^{2+}-dependent cell signalling through calmodulin-activated protein phosphatase and protein kinases minireview series. J. Biol. Chem. *276*, 2311–2312.

Sumi, M., Kiuchi, K., Ishikawa, T., Ishii, A., Hagiwara, M., Nagatsu, T., and Hidaka, H. (1991). The newly synthesized selective Ca^{2+}/calmodulin dependent protein kinase II inhibitor KN-93 reduces dopamine contents in PC12h cells. Biochem. Biophys. Res. Commun. *181*, 968–975.

Sze, H., Liang, F., Hwang, I., Curran, A.C., and Harper, J.F. (2000). Diversity and regulation of plant Ca^{2+} pumps: insights from expression in yeast. Annu. Rev. Plant Physiol. Plant Mol. Biol. *51*, 433–462.

Verde, F., Dogterom, M., Stelzer, E., Karsenti, E., and Leibler, S. (1992). Control of microtubule dynamics by cyclin A- and cyclin B-dependent kinases in *Xenopus* egg extracts. J. Cell Biol. *118*, 1097–1108.

Walczak, C.E. (2000). Microtubule dynamics and tubulin interacting proteins. Curr. Opin. Cell Biol. *12*, 52–56.

Weber, I., Gruber, C., and Steinberg, G. (2003). A class-V myosin required for mating, hyphal growth, and pathogenicity in the dimorphic plant pathogen *Ustilago maydis*. Plant Cell *15*, 2826–2842.

Wedlich-Söldner, R., Bölker, M., Kahmann, R., and Steinberg, G. (2000). A putative endosomal t-SNARE links exo- and endocytosis in the phytopathogenic fungus *Ustilago maydis*. EMBO J. *19*, 1974–1986.

Wedlich-Söldner, R., Schulz, I., Straube, A., and Steinberg, G. (2002a). Dynein supports motility of endoplasmic reticulum in the fungus *Ustilago maydis*. Mol. Biol. Cell. *13*, 965–977.

Wedlich-Söldner, R., Straube, A., Friedrich, M.W., and Steinberg, G. (2002b). A balance of KIF1A-like kinesin and dynein organizes early endosomes in the fungus *Ustilago maydis*. EMBO J. *21*, 2946–2957.

Willins, D.A., Xiang, X., and Morris, N.J. (1995). An alpha tubulin mutation suppresses nuclear migration mutations in *Aspergillus nidulans*. Genetics *141*, 1287–1298.

Yang, P., Diener, D.R., Rosenbaum, J.L., and Sale, W.S. (2001). Localization of calmodulin and dynein light chain LC8 in flagellar radial spokes. J. Cell Biol. *153*, 1315–1326.

Yoshida, T., Toda, T., and Yanagida, M. (1994). A calcineurin-like gene *ppb1*+ in fission yeast: mutant defects in cytokinesis, cell polarity, mating and spindle pole body positioning. J. Cell Sci. *107*, 1725–1735.